Supporting information for

A Goldilocks Energy Minimum: Peptide-based Reversible Aggregation and Biosensing

Wonjun Yim[1], Maurice Retout[2], Amanda A. Chen[2], Chuxuan Ling[2], Lubna Amer[1], Zhicheng Jin[2], Yu-Ci Chang[1], Saul Chavez[2], Karen Barrios[2], Benjamin Lam[2], Zhi Li[3], Jiajing Zhou[2], Lingyan Shi[3], Tod A. Pascal[2], and Jesse V. Jokerst[1,2,4*]

Correspondence to: jjokerst@eng.ucsd.edu

[1] Materials Science and Engineering Program, University of California San Diego, La Jolla, CA, 92093, USA

[2] Department of Nanoengineering, University of California San Diego, La Jolla, CA, 92093, USA

[3] Department of Bioengineering, University of California San Diego, La Jolla, CA, 92093, USA

[4] Department of Radiology, University of California San Diego, La Jolla, CA, 92093, USA

This PDF file includes:

Materials and Methods

Materials

Gold(III) chloride hydrate ($HAuCl_4 \cdot 3H_2O$, ≥99.9%), sodium citrate tribasic dihydrate (>99%), Trizma® base (>99.9%), Trizma® hydrochloride (>90%), DL-dithiothreitol (DTT, >99%), TFA (ReagentPlus®, 99%) trifluoroacetic acid (TFA, HPLC grade, >99%), piperidine (ReagentPlus®, 99%), trypsin, thrombin (from human plasma), hemoglobin human (lyophilized powder), albumin from bovine serum (BSA) and automation compatible syringe filters (hydrophilic PTFE, 0.45 µm) were purchased from Sigma-Aldrich (St Louis MO). Pyridine (ACS certified), acetic anhydride (ACS certified), thioanisole (>99%), 2,2′-(ethylenedioxy)diethanethiol (EDDET, 95%), N,N-diisopropylethylamine (DIPEA, >99%), and triisopropylsilane (TIPS, >98%) were purchased from Tokyo Chemical Industry Co., Ltd (TCI). Sodium chloride (NaCl, certified ACS), urea (certified ACS), and hydrochloric acid (certified ACS) were purchased from Fisher Chemical (Waltham, MA). N,N–dimethylformamide (DMF), acetonitrile (ACN, HPLC grade), ethyl ether (certified ACS), methylene chloride (DCM, certified ACS), dimethyl sulfoxide (DMSO, certified ACS), and uranyl acetate solution 2% were purchased from Fisher Scientific (Hampton, NH). Fmoc-Rink amide MBHA resin (0.67 mmol/g, 100-150 mesh), Fmoc-protected amino acids, and hexafluorophosphate benzotriazole tetramethyl uranium (HBTU) were purchased from AAPPTec, LLC (Louisville, KY). Silver nanoparticles (AgNPs, 20 nm) were purchased from Nanocomposite Inc. Disposable reaction vessel and the pressure caps for peptide-resin cleavage were purchased from Torviq Inc (Tucson, AZ). The recombinant SARS-CoV-2 main protease (M^{pro}) was expressed using the M^{pro} plasmid provided by Prof. Rolf Hilgenfeld, University of Lübeck (Germany) and purified by following method.[1] The purified M^{pro} was stored at –80 ºC in 20 mM Tris-HCl, pH 8.0, 150 mM NaCl, 1mM DTT, and 5% glycerol. M^{pro} inhibitor GC376 was purchased from Selleckchem. Human saliva and α-amylase (400 U/mL) were purchased from Lee Biosolutions (Maryland Heights, MO). The exhaled breath condensation (EBC) was obtained from healthy volunteers (COVID-negative) using a Rtube set-up (from Respiratory Research Inc.) with an IRB-approved protocol. The SealPlate® film (MKCS0276) was purchased from EXCEL Scientific. All reagents were used without further purification. Deionized water (18.2 MΩ·cm) purified with a Milli-Q Academic water purification system was used to make aqueous solutions. Glassware and stir bars were cleaned with aqua regia and washed with DI water before use.

Methods

1.1. Peptide synthesis

Peptides were synthesized based on Fmoc-SPPS (solid-phase peptide synthesis) on a Rink-amide-MBHA-resin (0.55 mmol/g, 200 mg for each sequence) using an automated Eclipse™ peptide synthesizer (AAPPTec, Louisville, KY). Amino acids were conjugated in nitrogen condition with 0.2 M Fmoc-amino acid (5 *equiv*) in 3 mL DMF, 0.2 M HBTU (5 *equiv*) in 3 mL DMF, 0.4 M DIPEA (7.5 *equiv*) in 3 mL DMF, and 20% (v/v) piperidine in 2 x 4 mL DMF for each cycle of

synthesis. The resulting peptides on the resin were transferred to the syringe filter (Torviq Inc), washed with two times of DMF (4 mL each) and four times of DCM (4 mL each), and dried under the vacuum condition (> 1h). N-terminal of the peptides was acetylated using the solution that contains 4 mL of DMF, 0.5 mL of Pyridine, and 0.5 mL of acetic anhydride. The resulting product was then washed with three times of DMF (3 mL) and three times of DCM (5 mL) and was vacuumed again to dry the sample. Lastly, the crude peptides were cleaved from the resins using a cocktail solution (5 mL) that includes 5 mL of TFA (83%), 300 µL of H_2O (5%), 300 µL of thioanisole (5%), 300 mg of phenol (5%), and 150 µL of EDDET (2%). The resins were incubated with the cocktail solution and rotated for 2 h. After the cleavage, the resin was filtered and the filtrate containing the crude peptides was precipitated using cold ethyl ether (10 mL, –20 ºC) and centrifuged three times (7,500 rpm, 5 minutes) to remove supernatants. The precipitated pellets were dried and re-suspended using 10 mL of ACN/H_2O mixtures (the percentage of ACN was controlled based on the solubility of the pellet (20–40% of ACN)). The peptides were purified by the reversed-phase HPLC (Shimadzu LC-40), confirmed by the ESI-MS, and stored in dry conditions at –20 ºC for future use.

1.2 Peptide purification

The crude peptides were purified using a Shimadzu LC-40 HPLC system established with a LC-40D solvent delivery module, photodiode array detector SPD-M40, and degassing unit DGU-403. 2 L of ACN (or H_2O) solution containing 0.05% TFA (HPLC grade) was prepared and degassed for the HPLC purification. 2 mL of the crude peptides dissolved in ACN/H_2O mixtures (10 mL, 20% of ACN and 80% of H_2O) was injected for each cycle. C4 column (5 µm, 20×200 mm) from SHMADZU was used for the purification and eluted with a flow rate of 5 mL/min over 30 min with a linear gradient from 10% to 95% of ACN in H_2O. The injection was monitored at 220 and 300 nm to collect the samples. The fractions which contained the target peptide confirmed by ESI-MS or/and MALDI were frozen at –80 ºC for 3 h, lyophilized, aliquoted, and dried for future use. All the purified peptides reached a purity of at least 90%. FreezeZone Plus 2.5 freeze dry system was used for the lyophilization.

1.3 Peptide aliquot

The concentration of each peptide was calibrated using a NanoDrop™ One UV-vis-spectrometer (Thermo Fisher Scientific, Waltham, MA). The 31-method adapted in Nanodrop™ was used to calibrate the peptide concentration except for tryptophan and tyrosine residues. The absorption of coefficient of ε_{205} (about 75 $mL \cdot mg^{-1} \cdot cm^{-1}$) was used for the measurement. The distilled water was used as a blank. After concentration measurement, the purified peptides were dried using a vacufuge and stored at –20 ºC for future use.

2. Limit of detection calculation

The limit of detection (LoD) was calibrated using the limit of blank (LoB).[2] The LoB defines the highest signal generated from a sample that includes no analyte. LoB could be calculated using the mean ($mean_{blank}$) and standard deviation (SD_{blank}) of a blank sample following equation:

$$LoB = mean_{blank} + 1.645\ (SD_{blank})$$

The LoD defines the lowest analyte concentration that can be differentiated from the LoB. LoD is calculated based on the LoB and standard deviation of the lowest concentration sample ($SD_{low\ concentration\ sample}$). Here, the LoD represents an analyte concentration at which 95% of measured samples are readily differentiated from the LoB while the remaining 5% can contain no analyte.

$$LoD = LoB + 1.645\ (SD_{low\ concentration\ sample})$$

Here, we used the dissociation peptide (*e.g.*, A18) and M^{pro} enzyme to measure the LoD in different conditions (PB buffer, saliva, and EBC). The fresh M^{pro} enzyme of the described amount was mixed with the parent peptide for 0.5h at 37 ºC. Then, the assay was transferred to the 96-well plate and incubated with RRK-induced gold aggregates. The homogeneity of plasmonic nanoparticles and media conditions can impact standard deviation and more monodisperse particles could improve the extent of color change and thus the LoD. At least three replicates of each experiment in saliva, EBC, and PB were performed on different days, respectively.

3. Specificity test

BSA (M_w: 66463 Da), hemoglobin (M_w: 64500 Da), thrombin (M_w: 37400 Da), α-amylase (1000U/ mL), M^{pro}, and human saliva were used for the specificity test. Briefly, the desired amounts of BSA, hemoglobin, thrombin, α-amylase and M^{pro} and human saliva were spiked into PB buffer (20 mM, pH 8.5) to reach the final concentration of 200 nM (200 U/ mL for α-amylase). Then, the parent A18 peptide (c_{final} = 50 μM) was mixed with different enzymes and conditions for 3h at 37 ºC. After 3h of incubation, the mixture was transferred into a 96-well plate, and 100 μL of the RRK-induced AuNP aggregates were injected for the specificity test. The absorbance of 520 nm and 700 nm were readout in the microplate reader at 37 ºC every 1 min for 1h. The ratiometric signal ($\lambda_{520/700}$) was recorded for data analysis. At least three replicates of each experiment were performed to measure the average and standard deviation.

4. Inhibitor test

GC376 inhibitor was used for the M^{pro} inhibitor assay. Briefly, the desired amounts of GC376 were pre-incubated with M^{pro} (200 nM) to reach final ratios; 1:5, 1:2, 1:1, 2:1, 5:1, and 10:1 indicate the molar ratio of inhibitor to M^{pro}. After the pre-incubation at room temperature for 15 min, the parent A18 peptide (c_{final} = 50 μM) was added and incubated for another 0.5h at 37 ºC. Then, the inhibitor

assay was transferred into a 96-well plate and incubated with 100 µL of the RRK-induced AuNP aggregates for the inhibitor test. The absorbance of 520 nm and 700 nm were readout in the microplate reader at 37 ºC every 1 min for 1h. The ratiometric signal ($\lambda_{520/700}$) at 1h was used for data analysis. The experiment was performed with three replicates in different conditions (PB, saliva, and EBC) to measure the average and standard deviation.

5. Colloidal stability test

The colloidal stability was tested using sodium chloride. Briefly, the peptide capped AuNPs was incubated with NaCl (0.5 to 2M) for 1h at room temperature. After the incubation, the assay was transferred into a 96-well plate, and absorbance from 300 to 900 nm was readout with the step size of 2 nm. Aggregation parameter (AP) was defined as follows:[3] $AP = (A - A_o)/A_o$, where A_o and A are the absorbance ratio ($\lambda_{520}/\lambda_{600}$) between 520 to 600 nm at the initial and final conditions. At least two replicates of each experiment were measured. The dissociated AuNPs by the A18 fragment was incubated in 50% Dulbecco's modified eagle medium, human saliva, urine, plasma and NaCl, respectively. The size was measured by DLS to check particle dispersion for Figure 5i.

6. Dissociation strategy using AgNPs

Briefly, RRK peptides were first used to aggregate AgNPs, changing the color from yellow to blue in 10 s. The dissociation peptides (*i.e.,* A18, Ace-CGGKKEEAVLQSGFR-Am) were incubated with M^{pro} at 37 ºC for 1h. After the incubation, the fragment peptide with different concentrations (from 50 to 200 µM) were used to dissociate AgNP aggregates. The ratiometric signal ($\lambda_{520/700}$) was readout in the microplate reader every 1min for 1h.

7. Investigation of RRK|Au and citrate|Au interactions using quantum mechanics (QM)

To investigate the RRK|Au and citrate|Au interaction energies, we performed QM computations using Quantum Espresso (QE)[4-5] package. For RRK, a relatively large molecule, we investigated RRK|Au interaction energy *via* computing the R group/K group binding on an Au(001). For citrate, we investigated citrate|Au interaction energy via computing the interaction of an entire citrate molecule on an Au(001). In addition, each model contained a corresponding number of Cl/H ions to ensure a charge neutral system. QM computations were performed with ultrasoft pseudopotentials, a cell box of (16.26, 12.195, 60) in (x,y,z), and a K-point grid (5,5,1). For each configuration, a molecule was initially placed near an Au(001) slab and gradually moved far away from an Au(001). Those QM energies were further applied in determining the Van der Waals parameters of RRK|Au and citrate|Au interactions for MD simulations.

8. General characterization

1. Transmission electron microscopy (TEM) images were obtained using a JEOL JEM-1400 Plus operating at 80 kV in the Nano3 cleanroom UCSD. TEM images were taken using an installed Gatan 4k digital camera in the machine. 2 µL of each diluted sample was dropped on the carbon grids and dried overnight for the sample preparation.
2. The hydrodynamic diameter and zeta potential (*i.e.,* surface charge) were measured using dynamic light scattering (DLS) with a Malvern Instrument Zetasizer ZS 90. The samples was diluted to measure the size and zeta potential. MQ water was used for the dilution.
3. Absorbance spectra were measuring using a BioTek Synergy H1 plate reader; 120 µL of each sample was measured in 96-well plates. Absorbance was collected from 400 to 800 nm with a step size of 2 nm. The sample absorption at the desired wavelength (*e.g.,* 520 and 700) was measured every 1 min for 1–3h. After injecting the samples into a 96-well plate, a film was attached to the plate to prevent solvent evaporation. The MQ water (or PB buffer) was used as a blank.
4. Fourier transform infrared (FTIR) data was obtained using A Bruker Tensor II FTIR spectrophotometer. The samples were dried overnight, and the dried solid sample was used for the FTIR measurement.
5. Multi-laser nanoparticle tracking analysis (M-NTA) measurement was performed using a ViewSizer 3000 (Horiba Scientific, CA, USA) to measure particle concentrations and size information.[6] 10 videos (8-bit) were recorded with a 30 fps for 10 s (*i.e.,* 300 frames for seconds), and the recorded videos were used to calibrate particle size. A quartz cuvette with a minimum sample volume of 0.8 mL was used for the measurement. 10 µL of each sample was diluted in 5 mL of DI water. The quartz cuvette and stirring bar were cleaned with DI water to minimize the background noises.
6. Peptide synthesis and cleavage was confirmed using electrospray ionization mass spectrometry (ESI-MS) *via* the Micromass Quattro Ultima mass spectrometer in the Molecular Mass facility (MMSF) at Chemistry and Biochemistry Department at UC San Diego. The sample for ESI-MS was prepared using 50% MeOH/H_2O mixtures. 2 µL of each sample was injected into the instrument three times independently to obtain ESI-MS data.
7. Peptide cleavage was confirmed using matrix assisted laser absorption ionization time of flight mass spectrometry (MALDI-TOF MS, Bruker Autoflex Max) in the MMSF at UC San Diego. 2 µL of each sample was mixed with 6 µL of HCCA matrix. Then, the mixture was placed on the plate and dried using a heat gun.
8. Raman spectra was measured by a Raman spectrometer connected to a confocal Raman microscope (XploRA PLUS, Horiba). A 532 nm diode line laser with a 50x objective lens (MPLN50X, Olympus) was used. A cooled charge coupled device (CCD) detector fitted to a 1800 grooves/mm grating spectrometer was used for signal detection. Raman spectra was collected at 30 s acquisition times with an accumulation of 2. Raman spectra was pre-processed using vector normalization and simplex normalized. The instrumental calibration was verified using the silicone line at 520 cm^{-1}.

Derjaguin-Landau-Verwey-Overbeak (DLVO theory)

The colloidal dispersion of AuNPs have been explained by DLVO theory where van der Waals (vdW) attraction is balanced by electrostatic repulsion, separating nanoparticles due to electric double layer (EDL). When breaking this balance by chemical bonding or ionic strength, Debye length (*i.e.*, electrostatic repulsive potential) decreases, leading to plasmon couplings (i.e., aggregation).[7]

$$U_{1-2}^{DLVO} = U_{1-2}^{vdW} + U_{1-2}^{EDL}$$

$$U_{1-2}^{vdW} = -\frac{A_H}{6}\left[\frac{8R_R^2}{h(R_R+h)} + \frac{8R_R^2}{(4R_R+h)} + ln\frac{h(8R_R+h)}{(4R_R+h)^2}\right]$$

$$U_{1-2}^{EDL} = 4\pi\varepsilon\varepsilon_0 R_R[\varphi_1\varphi_2\exp(-\kappa h) - \frac{1}{4}({\varphi_1}^2 + {\varphi_2}^2\exp(-2\kappa h)]$$

$$\kappa^{-1} = \sqrt{\frac{\varepsilon\varepsilon_0 k_B T}{2N_A I e^2}}$$

where $U_{1\text{-}2}$ is the total interaction energy between AuNP #1 and AuNP #2 in water as a function of interaction distance (h). $U_{1\text{-}2}^{vdW}$ is the vdW interaction energy and $U_{1\text{-}2}^{EDL}$ is the electrostatic interaction energy. A_H is Hamaker constant (intrinsic property) of the two interacting AuNPs. R_R is reduced particle radius, e is a unit charge (1.602×10^{-19}), φ_1 and φ_2 are surface potentials (mV) of two interacting AuNPs. N_A is Avogadro's number (6.02×10^{23} mol^{-1}), ε is dielectric constant of water (78.5), ε_0 is dielectric permittivity of a vacuum (8.854×10^{-12} C/(V·M)) and I is the ionic strength. κ^{-1} is a Debye length (mm) which represent the thickness of EDL as a result of the ionic strength and electrolytes.[7]

In conclusion, EDL energy barriers between two AuNPs could decrease when RRK peptide was introduced, inducing particle aggregation. The particle dissociation could occur likely due to the increased steric repulsion, hydrophilicity, and recovered electrostatic repulsion.

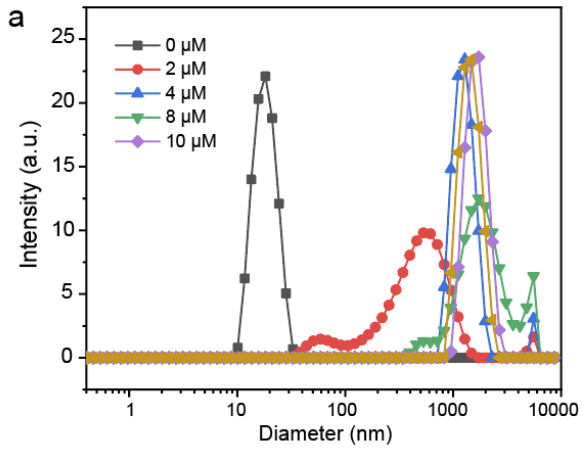

Figure S1: RRK-induced AuNP aggregates
RRK peptides with 2 to 10 µM were used to aggregate AuNPs. DLS data showed that the size of citrate-coated AuNPs were aggregated by the RRK peptides.

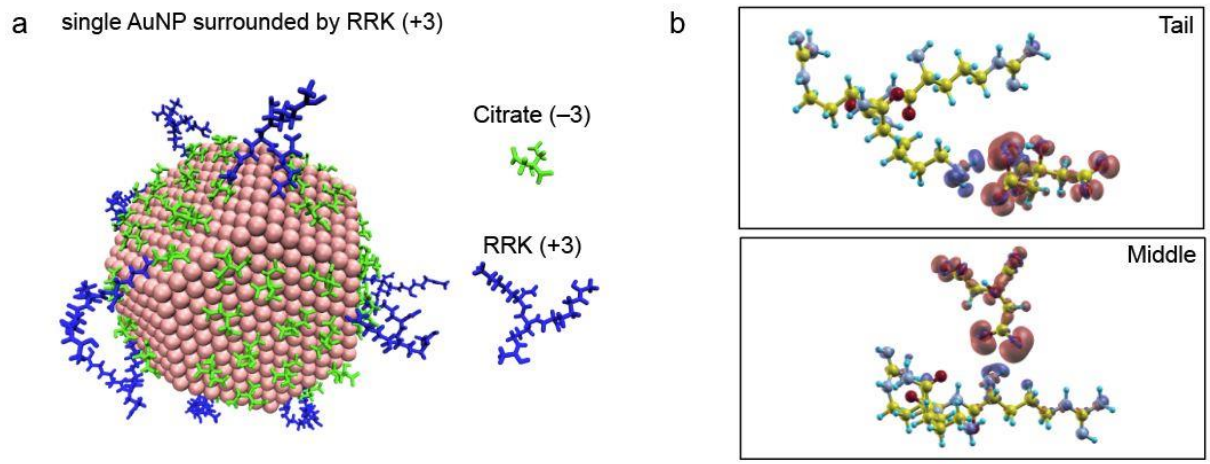

Figure S2: Interactions between RRK and citrate molecules
a, Molecular dynamics (MD) snapshots of a citrate-coated Au nanoparticle system after adding RRK molecules. Na ions, Cl ions, and water molecules are not shown for clarification. **b**, Simulated charge density indicated that molecular interactions between RRK peptides and citrate readily occurred at a tail portion rather than the middle portion due to atomic charge effects.

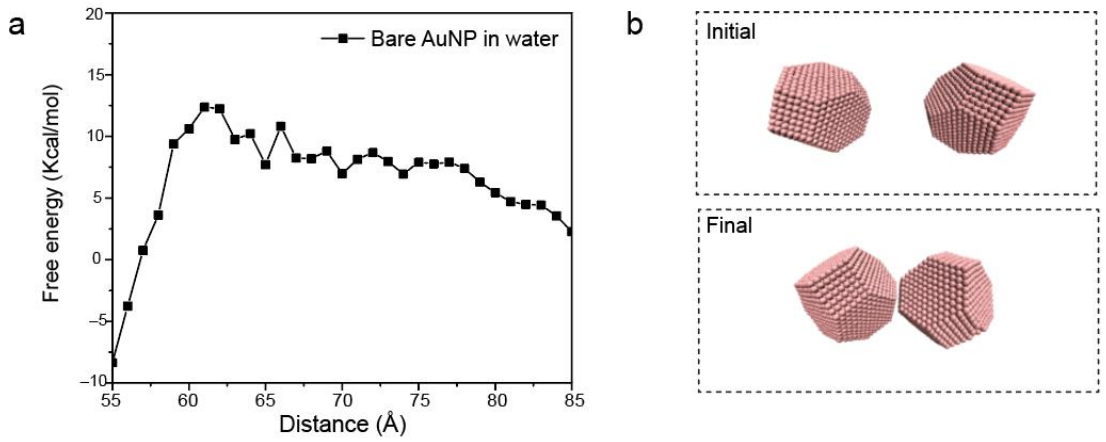

Figure S3: Free energy investigation as a function of AuNP distance
a, SMD simulation for a system with bare two AuNPs in water. The x axis indicates the center of mass between two bare AuNPs. Without citrate on AuNPs, free energy decreased as a function of increased VdW interactions. **b,** The initial and final snapshots of two bare AuNPs are shown. The water molecules are not shown for clarification.

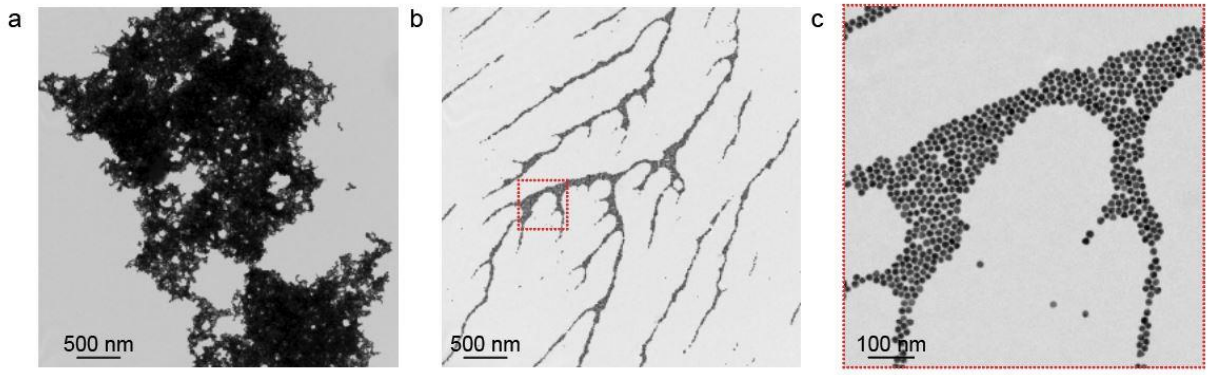

Figure S4: TEM images of AuNP aggregates and particle dissociations
a, AuNP aggregates induced by RRK peptides. **b**, After adding the dissociation peptides (A1, Ace-EEKKPPC-Am), the aggregated AuNPs were re-dispersed. **c**, High-magnified TEM image in the red-dotted box in panel (**b**). 10 μM of RRK peptide was used to induce particle aggregation. 150 μM of the A1 peptide was used for particle dissociation.

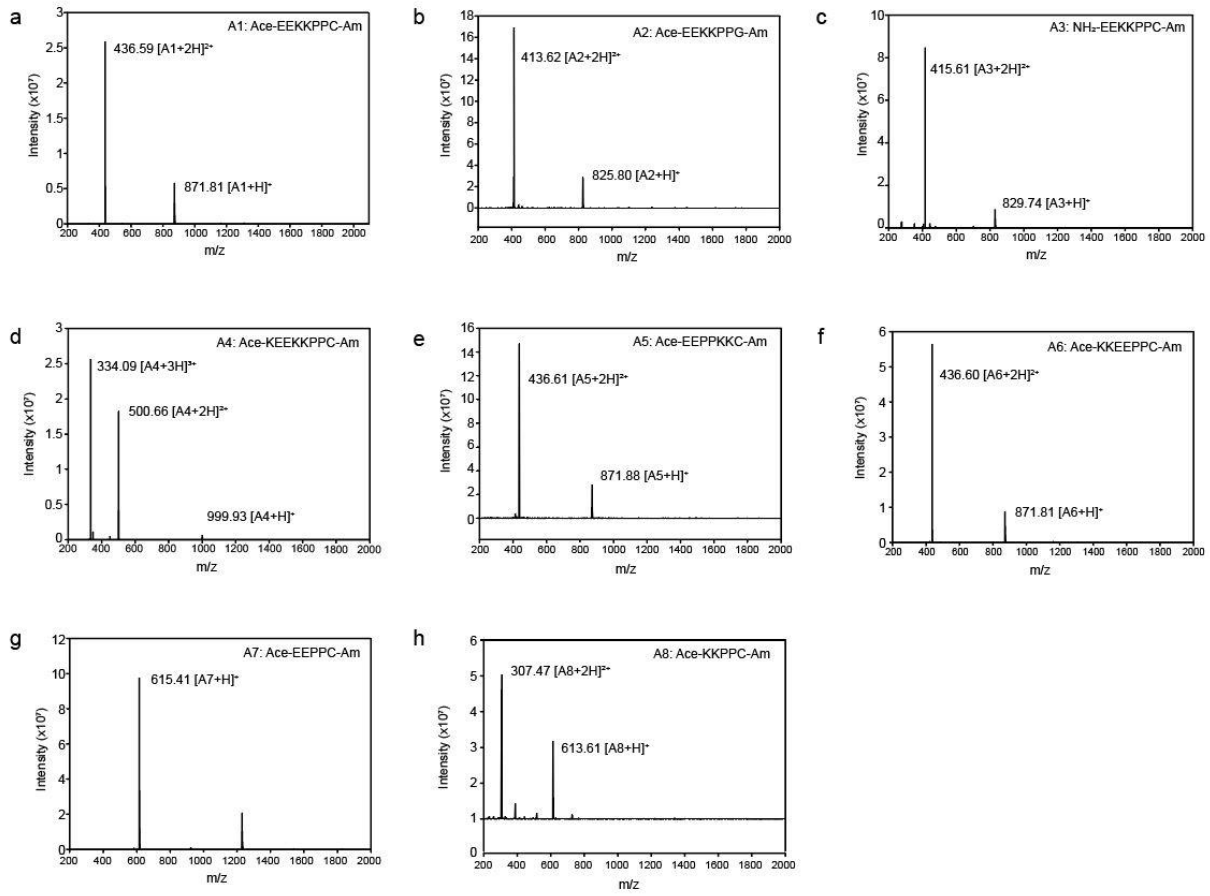

Figure S5: ESI-MS data of eight peptide sequences (A1–A8) to define the role of amino acid in dissociation peptide

ESI-MS data of (**a)** A1 (Ace-EEKKPPC-Am), **(b)** A2 (Ace-EEKKPPG-Am), **(c)** A3 (NH_2-EEKKPPG-Am), **(d)** A4 (Ace-KEEKKPPC-Am), **(e)** A5 (Ace-KEEPPKKC-Am), **(f)** A6 (Ace-KKEEPPC-Am), **(g)** A7 (Ace-EEPPC-Am), and **(h)** A8 (Ace-KKPPC-Am).

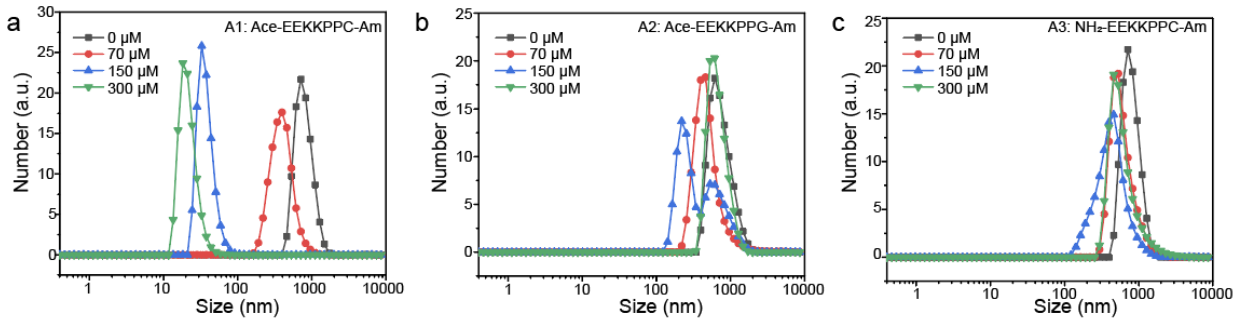

Figure S6: The role of cysteine and acetylation in the particle dissociation
a, A1 peptide with the concentration of 150 and 300 μM dissociated AuNP aggregates while A2 peptide (i.e., without cysteine) (**b**) and A3 (free amine at the N-terminus) (**c**) failed to dissociate AuNP aggregates. These results indicate that the cysteine residue in the C-terminus is required for Au-S binding. In addition, the positively charged peptides (*e.g.*, A3, and A4) cannot dissociate AuNP aggregates.

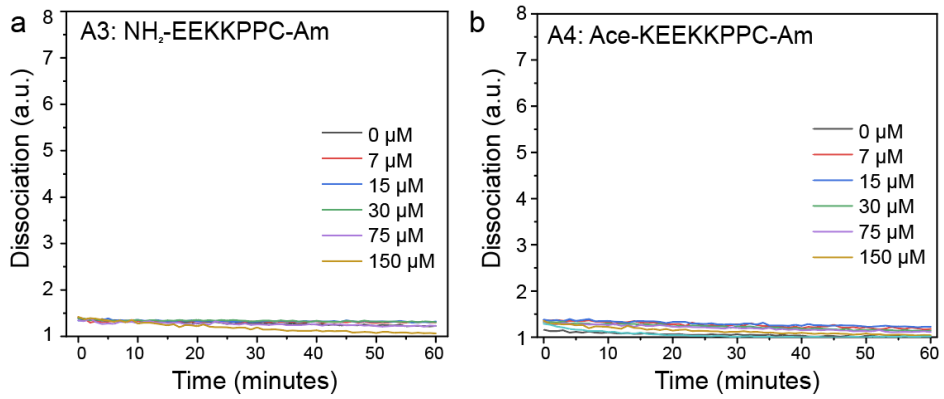

Figure S7: Free amine at N terminus prevents particle dissociation
To further confirm that free amine at N terminus can inversely impact on particle dissociation, we synthesized the A4 peptide which contains Lys at the C terminus. Not surprisingly, the A3 (**a**) and A4 (**b**) peptide failed to dissociate AuNP aggregates, meaning that positive charged peptides are incapable of dissociating AuNP aggregates.

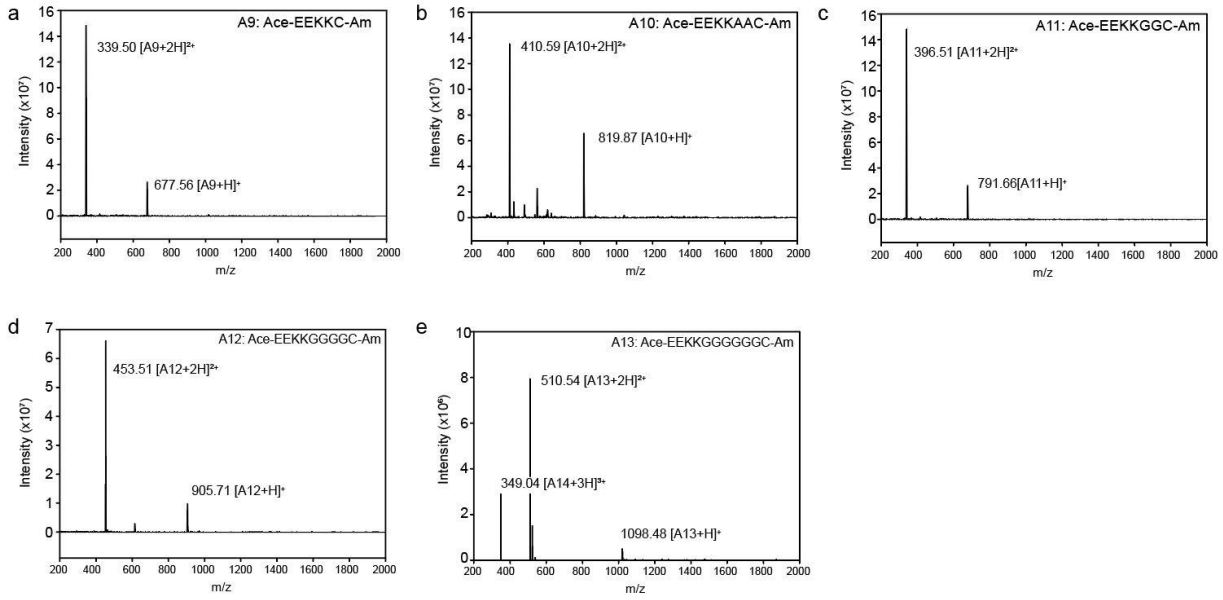

Figure S8: ESI-MS data A9–A13 peptides
ESI-MS data of (**a)** A9 (Ace-EEKKC-Am), **(b)** A10 (Ace-EEKKAAG-Am), **(c)** A11 (Ace-EEKKGGC-Am), **(d)** A12 (Ace-EEKKGGGGC-Am), **(e)** A13 (Ace-EEKKGGGGGGC-Am).

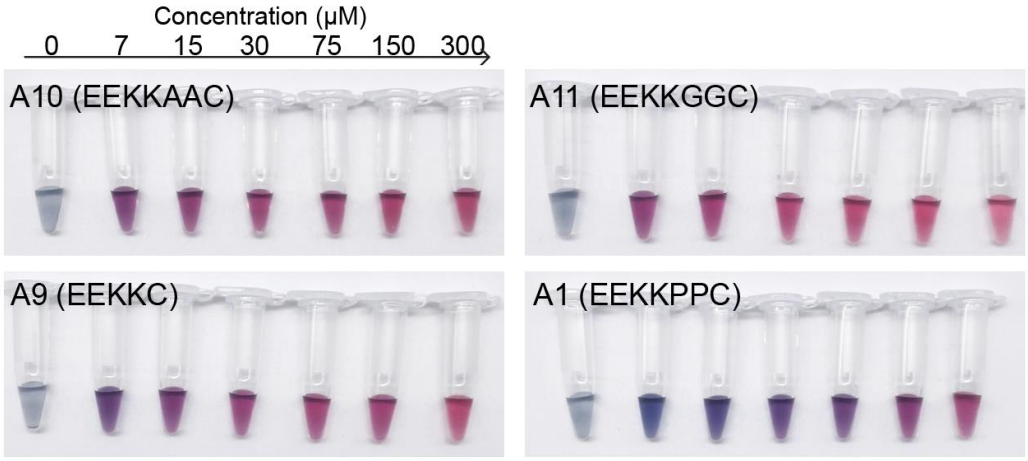

Figure S9: Photographs of the dissociated AuNPs by A1, A9, A10, A11 peptides
The AuNP aggregates were dissociated using A1 (Ace-EEKKPPC-Am), A9 (Ace-EEKKC-Am), A10 (Ace-EEKKAAC-Am), A11 (Ace-EEKKGGC-Am). The color changed from blue to red due to the particle dissociation.

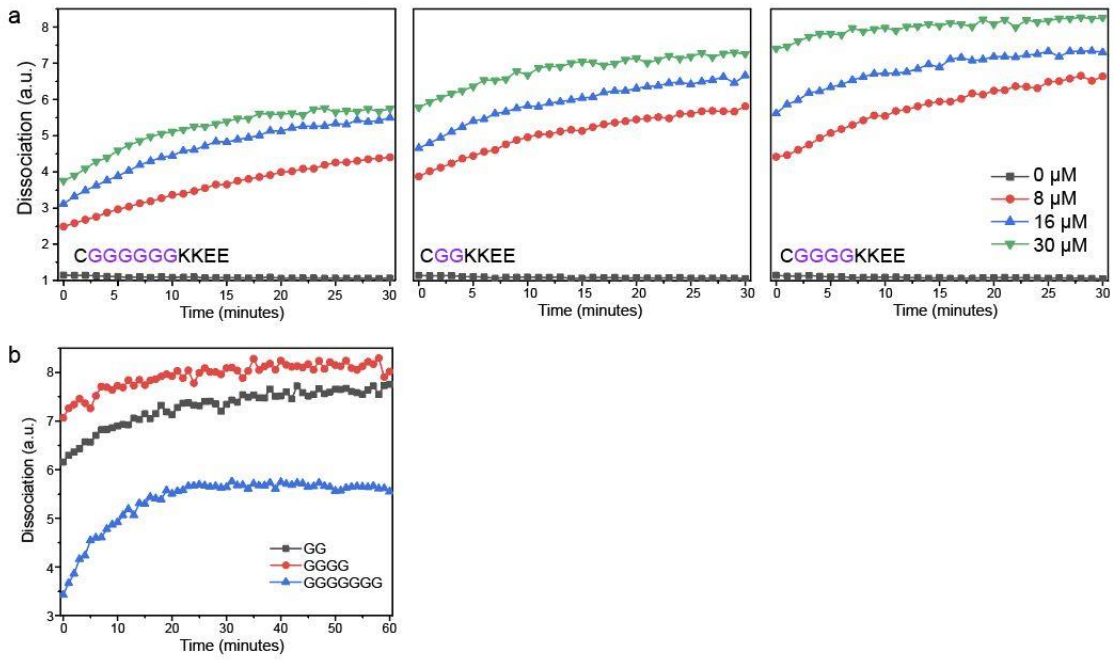

Figure S10: Impact of spacer lengths on the particle dissociation

a, Time-dependent particle dissociations using A11 (Ace-EEKKGGC-Am), A12 (Ace-EEKKGGGGC-Am), and A13 (Ace-EEKKGGGGGGC-Am) peptides. The results showed that spacer length can impact the dissociation capacity of the peptide. **b,** The particle dissociation was attenuated likely due to the increased steric hinderance by length.

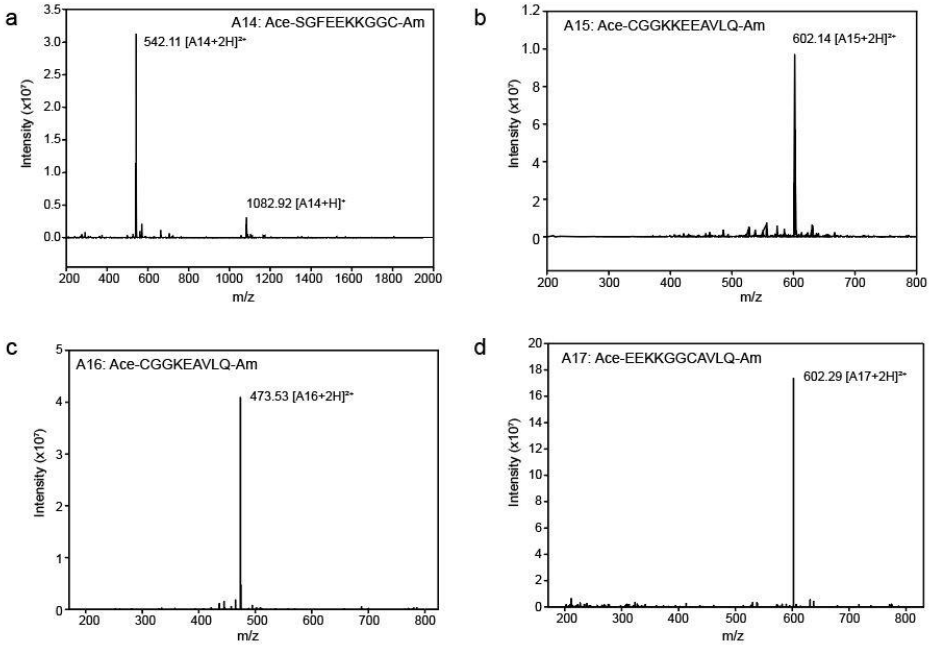

Figure S11: ESI-MS data of A14–A17 peptides
ESI-MS data of **(a)** A14 (Ace-SGFEEKKGGC-Am), **(b)** A15 (Ace- CGGKKEEAVLQ-Am), **(c)** A16 (Ace-CGGKEAVLQ-Am), and **(d)** A17 (Ace- EEKKGGCAVLQ-Am).

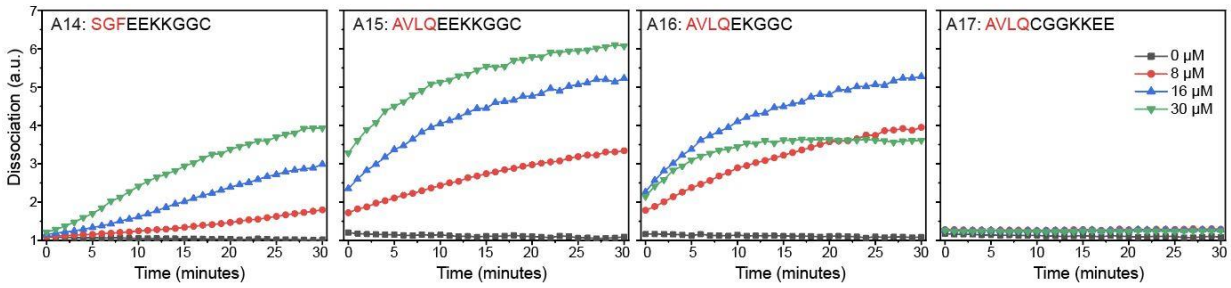

Figure S12: Impact of the fragment sequence, length, and the location of cysteine on the particle dissociation

Time-dependent particle dissociations using the A14, A15, A16, and A17 peptides, respectively. M^{pro} fragments (which are SGF and AVLQ) could attenuate the dissociation efficiency. The SGF fragment more reduced the dissociation capacity than AVLQ fragment likely due to strong hydrophobicity of Phe (F) amino acid. It is notable that the location of Cys is also important to dissociate AuNP aggregates. For example, the Cys at the N-terminus (i.e., A15) dissociated AuNP aggregates while the Cys in the middle (i.e., A17) failed to dissociate AuNP aggregates. This is likely because ligand architecture could impact on grafting density of peptide on AuNPs. The Cys in the middle could have less passivation layer which prevents particle dissociation.[8]

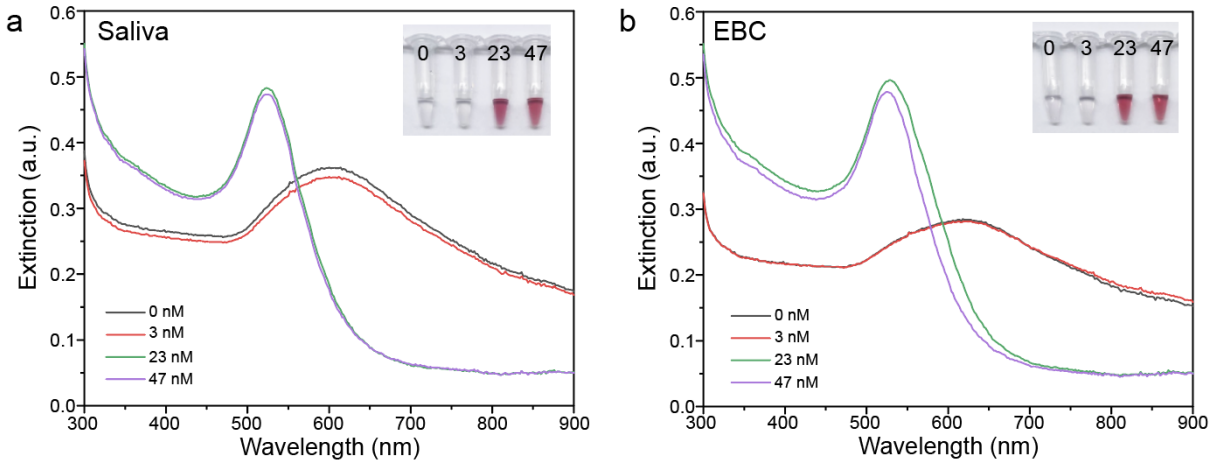

Figure S13: Dissociation strategy applied in saliva and EBC
M^{pro} cleaved the dissociation peptides (*i.e.*, A18, Ace-CGGKKEEAVLQSGFR-Am) in saliva (**a**), EBC (**b**), and the fragments dissociated AuNPs, changing color to reddish. The UV-vis spectrum showed the dissociated AuNPs with the different M^{pro} concentrations.

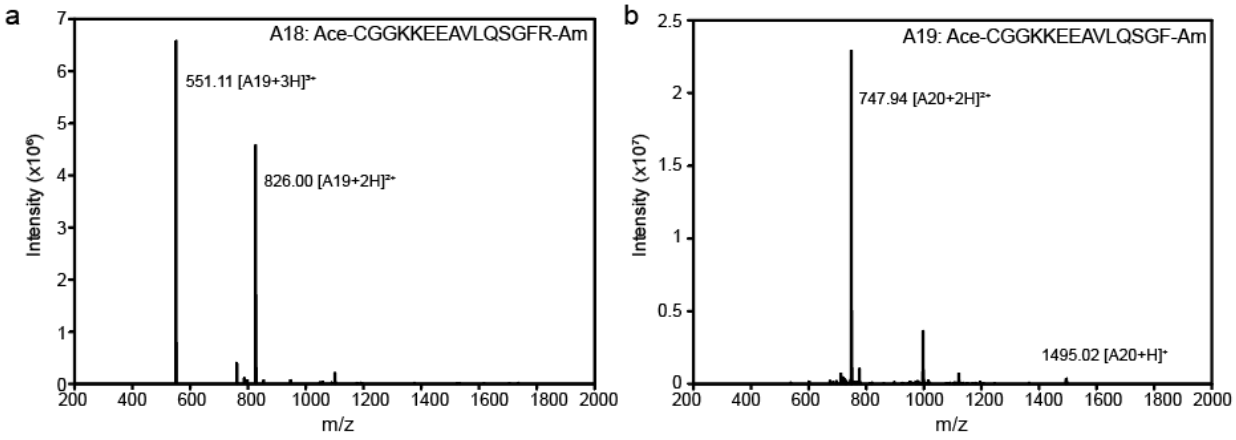

Figure S14: ESI-MS data of A18–19 peptides
ESI-MS data of (**a**) A18 (Ace-CGGKKEEAVLQSGFR-Am), **(b)** A19 (Ace-CGGKKEEAVLQSGF-Am).

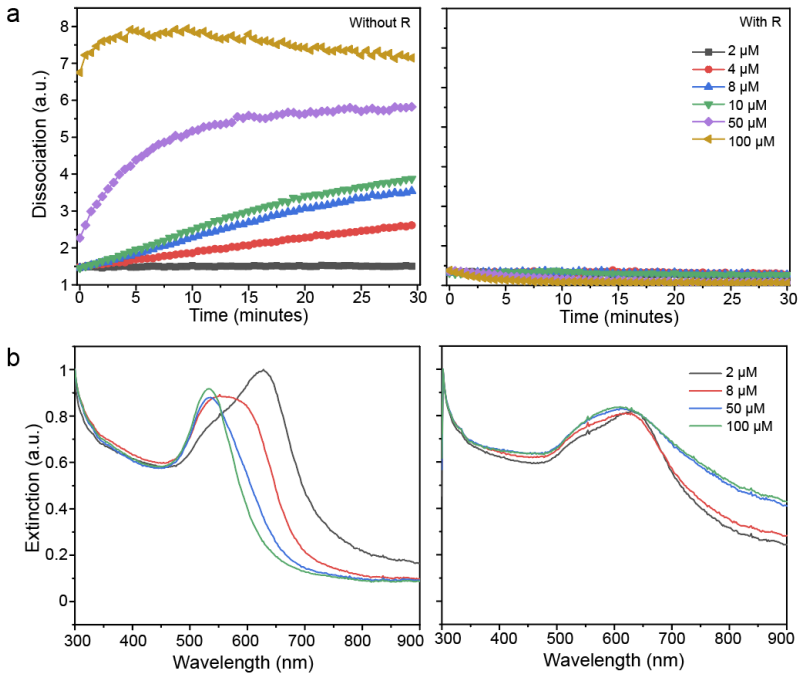

Figure S15: Arg residue at the C terminus for charge-screening

To prevent false positive, the dissociation peptide was charge-screened using Arg at the C terminus. AuNP aggregates were incubated with the different concentrations (from 2 to 100 μM) of A18 (with R) and A19 (without R) peptides. **a,** Time-dependent particle dissociations and their UV-vis spectrum (**b**). The results showed that the A19 peptide dissociated AuNP aggregates without M^{pro} (i.e., false positive) while A18 peptide which included Arg residue prevents the false positive.

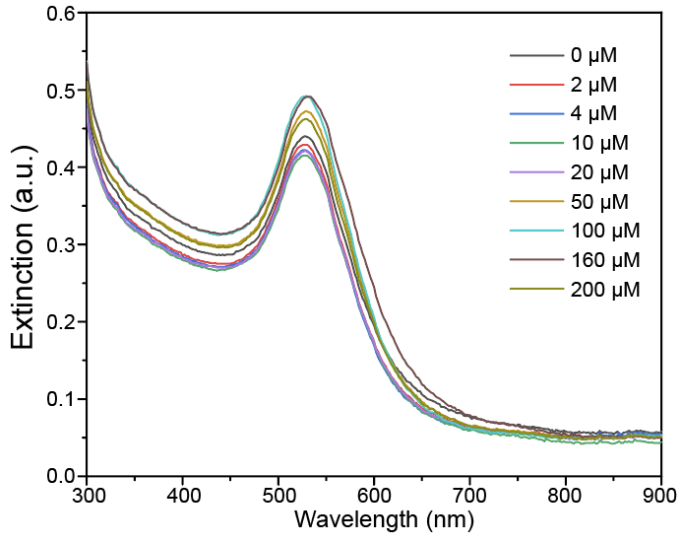

Figure S16: Impact of the SGFR fragment on particle dissociation
After M^{pro} cleavage, the A18 fragments (*i.e.*, CGGKKEEAVLQ) dissociated AuNP aggregates. SGFR showed negligible impact on particle dissociation. UV-vis spectrum showed that the dissociated AuNPs by the A18 fragments maintained high colloidal stability in the presence of SGFR fragments from 2 to 200 μM.

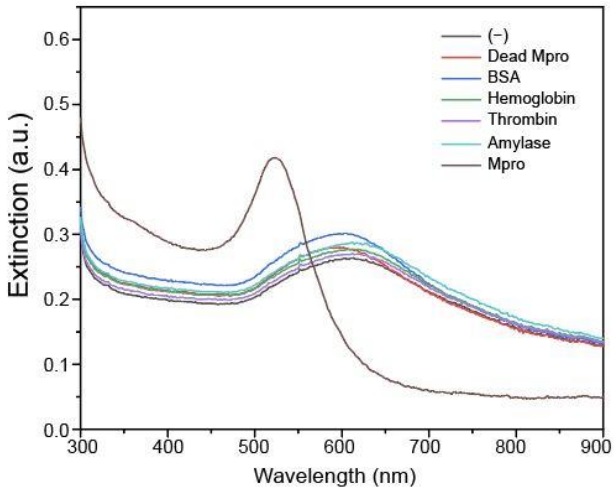

Figure S17: UV-vis spectrum of the specificity test

The inactive M^{pro} (incubated 60 ºC for 3h), BSA, hemoglobin, thrombin, α-amylase, saliva and M^{pro} were incubated with the dissociation peptide (*i.e.*, A18) for 1h at 37 ºC. After then, AuNP aggregates were used for the specificity test. The UV-vis spectrum showed that only M^{pro} dissociated AuNP aggregates due to the release of the dissociation peptides while other enzymes and proteins did not induce the particle dissociations.

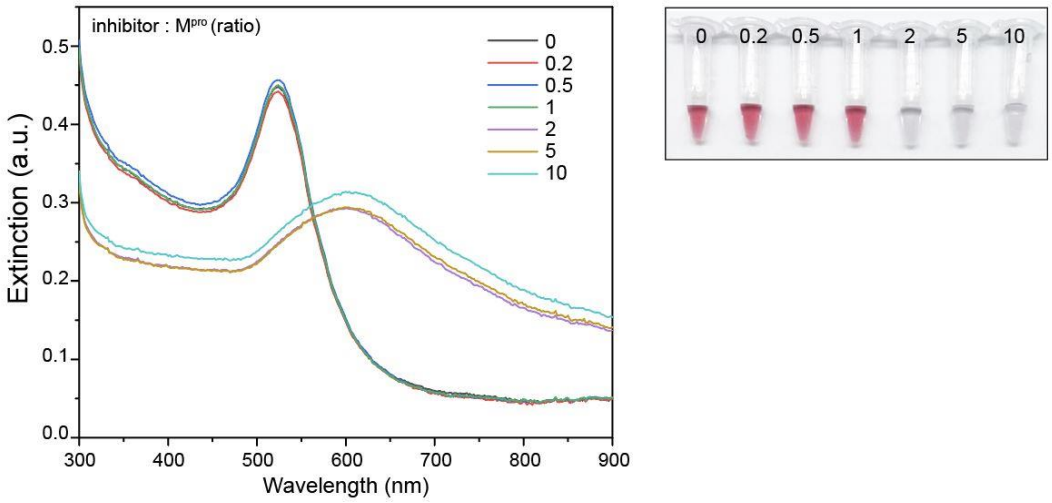

Figure S18: UV-vis spectrum of the inhibition test

The GC376 inhibitor was incubated with M^{pro} for the inhibition test. The 0, 0.2, 0.5, 1, 2, 5, and 10 represent the ratio between inhibitor to M^{pro} (200 nM). The results showed that GC376 inhibited M^{pro} proteolytic activity, preventing particle dissociation.

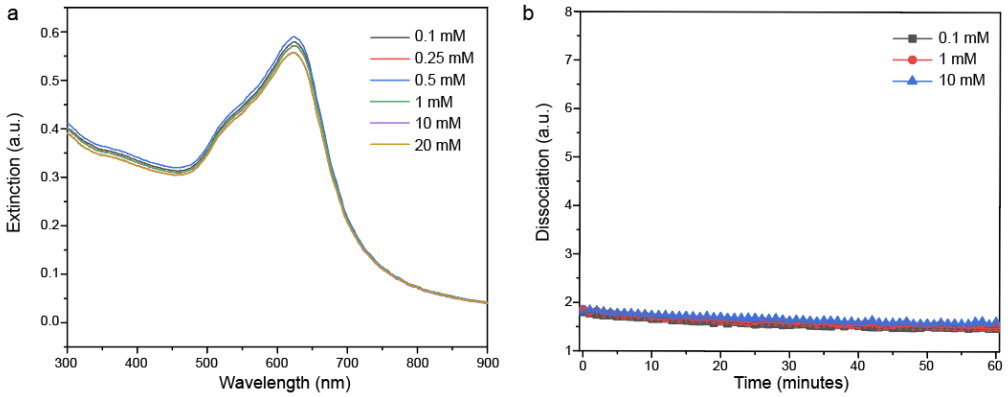

Figure S19: GC376 inhibitor with AuNP aggregates
The GC376 inhibitor (from 0.1 to 20 mM) was incubated with AuNP aggregates. UV-vis spectrum (**a**) and time-dependent particle dissociation (**b**) showed that the inhibitor itself had no impact on the particle dissociation.

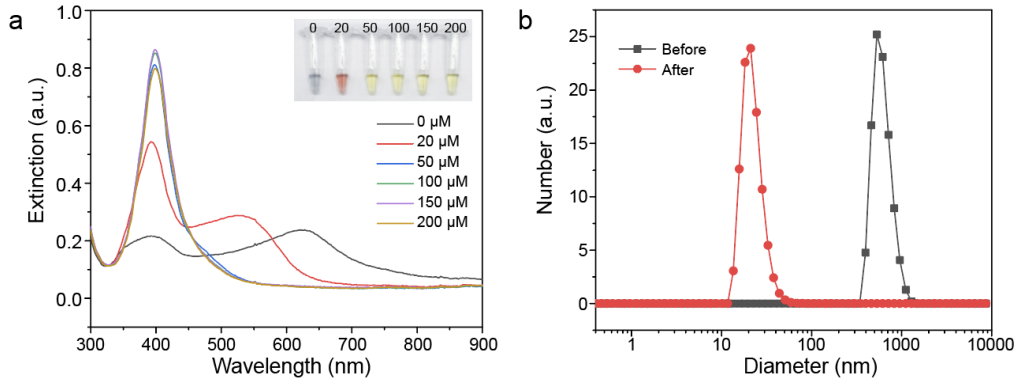

Figure S20: Dissociation strategy using 20 nm AgNPs

a, UV-vis spectrum and (**b**) DLS data of the dissociated AgNP aggregates using the dissociation peptides. The A18 fragments released by M^{pro} cleavage (20–200 μM) were used for the dissociation test. These results showed that our dissociation strategy could be applied using AgNPs which provide a broader absorption shift (from blue to yellow).

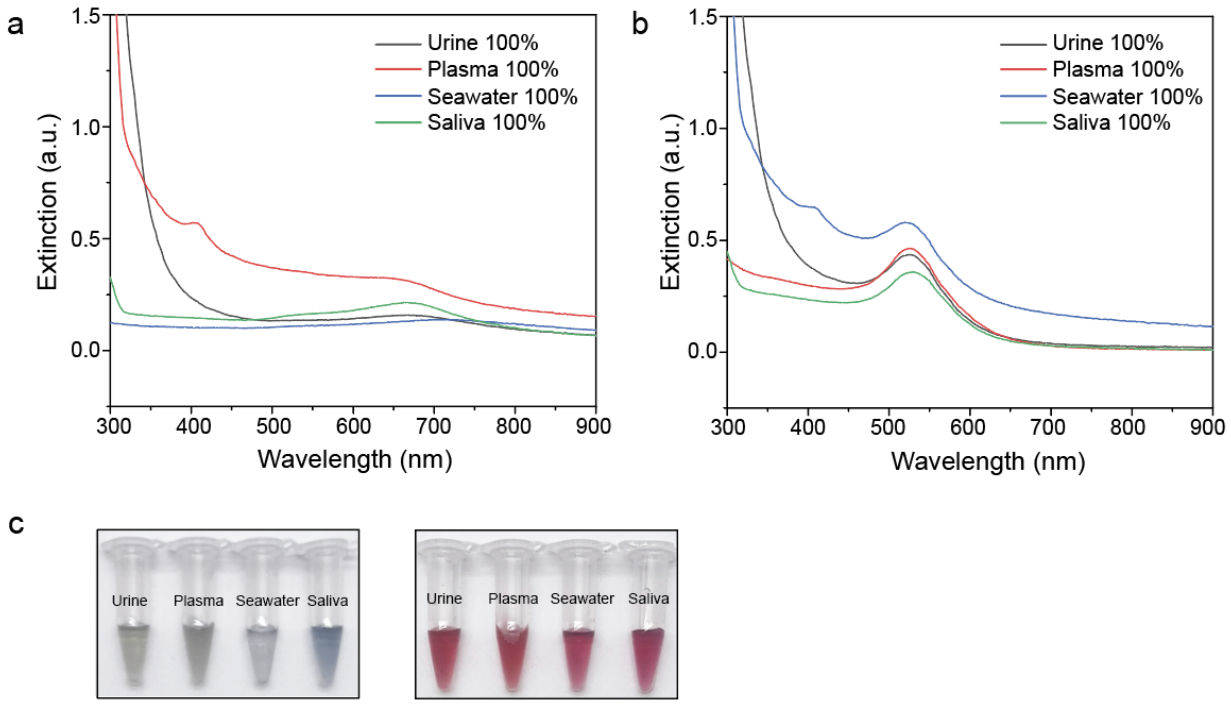

Figure S21: Particle dissociation in 100% human urine, plasma, seawater, and saliva
UV-vis spectrum of AuNP aggregates (**a**) and the dissociated AuNPs (**b**) after adding dissociation peptide (*i.e*, A11) in 100% human urine, plasma, seawater, and saliva. **c**, Photographs show that our dissociation peptide can re-disperse AuNP aggregates, offering color changes from blue to red in diverse matrixes.

References

(1) Zhang, L.; Lin, D.; Sun, X.; Curth, U.; Drosten, C.; Sauerhering, L.; Becker, S.; Rox, K.; Hilgenfeld, R. Crystal Structure of SARS-CoV-2 Main Protease Provides a Basis for Design of Improved α-Ketoamide Inhibitors. *Science* **2020,** *368* (6489), 409-412.
(2) Armbruster, D. A.; Pry, T. Limit of Blank, Limit of Detection and Limit of Quantitation. *Clin. Biochem. Rev.* **2008,** *29* (Suppl 1), S49.
(3) Lévy, R.; Thanh, N. T.; Doty, R. C.; Hussain, I.; Nichols, R. J.; Schiffrin, D. J.; Brust, M.; Fernig, D. G. Rational and Combinatorial Design of Peptide Capping Ligands for Gold Nanoparticles. *J. Ame. Chem. Soc.* **2004,** *126* (32), 10076-10084.
(4) Giannozzi, P.; Baroni, S.; Bonini, N.; Calandra, M.; Car, R.; Cavazzoni, C.; Ceresoli, D.; Chiarotti, G. L.; Cococcioni, M.; Dabo, I.; Corso, A. D.; Gironcoli, S. d.; Fabris, S.; Fratesi, G.; Gebauer, R.; Gerstmann, U.; Gougoussis, C.; Kokalj, A.; Lazzeri, M.; Martin-Samos, L.; Marzari, N.; Mauri, F.; Mazzarello, R.; Paolini, S.; Pasquarello, A.; Paulatto, L.; Sbraccia, C.; Scandolo, S.; Sclauzero, G.; Seitsonen, A. P.; Smogunov, A.; Umari, P.; Wentzcovitch, R. M. QUANTUM ESPRESSO: a modular and open-source software project for quantum simulations of materials. *Journal of Physics: Condensed Matter* **2009,** *21*, 395502.
(5) Giannozzi, P.; Andreussi, O.; Brumme, T.; Bunau, O.; Nardelli, M. B.; Calandra, M.; Car, R.; Cavazzoni, C.; Ceresoli, D.; Cococcioni, M.; Colonna, N.; Carnimeo, I.; Corso, A. D.; Gironcoli, S. d.; Delugas, P.; Jr, R. A. D.; Ferretti, A.; Floris, A.; Fratesi, G.; Fugallo, G.; Gebauer, R.; Gerstmann, U.; Giustino, F.; Gorni, T.; Jia, J.; Kawamura, M.; Ko, H.-Y.; Kokalj, A.; Küçükbenli, E.; Lazzeri, M.; Marsili, M.; Marzari, N.; Mauri, F.; Nguyen, N. L.; Nguyen, H.-V.; Otero-de-la-Roza, A.; Paulatto, L.; Poncé, S.; Rocca, D.; Sabatini, R.; Santra, B.; Schlipf, M.; Seitsonen, A. P.; Smogunov, A.; Timrov, I.; Thonhauser, T.; Umari, P.; Vast, N.; Wu, X.; Baroni, S. Advanced capabilities for materials modelling with Quantum ESPRESSO. *J. Phys.: Condens. Matter* **2017,** *29*, 465901.
(6) McElfresh, C.; Harrington, T.; Vecchio, K. S. Application of a Novel New Multispectral Nanoparticle Tracking Technique. *Meas. Sci. Technol.* **2018,** *29* (6), 065002.
(7) Zhang, W. Nanoparticle aggregation: principles and modeling. *Nanomater.* **2014**, 19-43.
(8) Nowinski, A. K.; Sun, F.; White, A. D.; Keefe, A. J.; Jiang, S. Sequence, Structure, and Function of Peptide Self-Assembled Monolayers. *J. Am. Chem. Soc.* **2012,** *134* (13), 6000-6005.